Journal of Cerebral Blood Flow & Metabolism (2015) 35, 543–553

www.jcbfm.com

ORIGINAL ARTICLE

Premyelinated central axons express neurotoxic NMDA receptors: relevance to early developing white-matter injury

Tahani Huria[1], Narasimha Murthy Beeraka[1], Badrah Al-Ghamdi[1] and Robert Fern[2]

Ischemic-type injury to developing white matter is associated with the significant clinical condition cerebral palsy and with the cognitive deficits associated with premature birth. Premyelinated axons are the major cellular component of fetal white matter and loss of axon function underlies the disability, but the cellular mechanisms producing ischemic injury to premyelinated axons have not previously been described. Injury was found to require longer periods of modelled ischemia than at latter developmental points. Ischemia produced initial hyperexcitability in axons followed by loss of function after Na^+ and Ca^{2+} influx. *N*-methyl-D-aspartate- (NMDA) type glutamate receptor (GluR) agonists potentiated axon injury while antagonists were protective. The NMDA GluR obligatory Nr1 subunit colocalized with markers of small premyelinated axons and expression was found at focal regions of axon injury. Ischemic injury of glial cells present in early developing white matter was NMDA GluR independent. Axons in human postconception week 18 to 23 white matter had a uniform prediameter expansion phenotype and postembedded immunogold labelling showed Nr1 subunit expression on the membrane of these axons, demonstrating a shared key neuropathologic feature with the rodent model. Premyelinated central axons therefore express high levels of functional NMDA GluRs that confer sensitivity to ischemic injury.

Journal of Cerebral Blood Flow & Metabolism (2015) **35,** 543–553; doi:10.1038/jcbfm.2014.227; published online 17 December 2014

Keywords: axon; glutamate; ischemia; white matter

INTRODUCTION

Glutamate is the major excitatory neurotransmitter of the central nervous system, acting upon a variety of metabotropic and ionotropic receptors. Among the ionotropic receptor class, *N*-methyl-D-aspartate-type glutamate receptors (GluRs) have unique properties that allow them to act as coincidence detectors, requiring both the presence of agonist and a depolarizing stimulus to evoke a signal in the postsynaptic cell. This is the case not only at synapses but also at the axon growth cone where receptor activation is a positive modulator of extension.[1] *N*-methyl-D-aspartate GluRs are also present in the axon cylinder neighboring the growth cone where their function is not known.[2–4] Axonal expression is highest during early white-matter development, before the onset of myelination.[5,6] Although axons that have yet to myelinate (premyelinated axons) are generally resistant to ischemic conditions,[7] they are the major cellular component of the fetal white matter that is subject to focal and diffuse ischemic-type injuries giving rise to cerebral palsy and cognitive deficits in premature infants; two large and untreatable patients cohorts.[8–10] A recent report highlighted the loss of unmyelinated axons in a fetal rabbit model of cerebral palsy, with a reduced number of myelinated axons at latter ages suggesting that the lost unmyelinated axons correspond to premyelinating axons.[11]

Expression of NMDA-type GluRs on oligodendrocyte processes results in high ischemia sensitivity in these structures,[12,13] but the significance of expression on the premyelinated axon cylinder is not known. Excitotoxicity has been reported in immature central axons that have initiated oligodendrocyte ensheathment,[14,15] but susceptibility to excitotoxic injury in the period in axon development before the consolidation of synapses and loss of axon growth cones has not previously been examined. Indeed, axon injury mechanisms in the period before the consolidation of synapses and loss of axon growth cones have not previously been investigated. We have examined the injury mechanism operating in these clinically significant structures and have confirmed expression of NMDA GluR on human mid-gestation periventricular white-matter axons.

MATERIALS AND METHODS

UK home office regulations were followed for all experimental work, which was conducted in accordance with the relevant guidelines and regulations. The animal welfare and ethics committee of the University of Leicester approved all the experimental protocols. Rat optic nerves (RONs) were dissected from Lister-hooded rats between postnatal day 0 and 4 (referred to as 'P2'), P8 or adult. Nerves were perfused with artificial cerebrospinal fluid (aCSF), composition (in mmol/L): NaCl, 126; KCl, 3; NaH_2PO_4, 2; $MgSO_4$, 2; $CaCl_2$, 2; $NaHCO_3$, 26; glucose, 10; pH, 7.45, bubbled with 5% CO_2/95% O_2 and maintained at 37°C. Zero-Ca^{2+}aCSF: $CaCl_2$ was omitted and 50 μmol/L EGTA was added. Zero-Na^+ aCSF: Na^+ was substituted with choline. For oxygen–glucose deprivation (OGD), aCSF was replaced by glucose-free aCSF prebubbled with 95% N_2/5% CO_2 for at least 60 minutes. The chamber atmosphere was switched to 5% CO_2/95% N_2 during OGD. Osmolarity of solutions was measured and adjusted as required. Data are mean ± s.e.m., significance determined by t-test or ANOVA as appropriate. Glutamate receptor antagonists were from Tocris (Bristol, UK), all other reagents were from Sigma (Gillingham, UK). Drug treatments were initiated 10 minutes before the onset of OGD and were washed out 10 minutes after OGD, followed by a further 50 minutes recovery period.

[1]Department of Cell Physiology and Pharmacology, University of Leicester, Leicester, UK and [2]Peninsula School of Medicine and Dentistry, University of Plymouth, John Bull Building, Research Way, Plymouth, UK. Correspondence: Professor R Fern, Peninsula School of Medicine and Dentistry, University of Plymouth, John Bull Building, Research Way, Plymouth PL6 8BU, UK.
E-mail: robert.fern@plymouth.ac.uk
Received 22 September 2014; revised 12 November 2014; accepted 19 November 2014; published online 17 December 2014

Electrophysiology

The electrophysiologic recording techniques have been described recently.[16] In brief, compound action potentials (CAPs) were evoked and recorded with glass electrodes and peak-to-peak amplitude was used to assess changes in axonal integrity (see Fern *et al*[7]). Compound action potentials were evoked via square-wave constant current pulses (Isostim A320, WPI, Sarasota, FL, USA), amplified (Cyber Amp 320, Axon Instruments, Sunnyvale, CA, USA), subtracted from a parallel differential electrode, filtered (low pass: 800 Hz), digitized (1401 mini, Cambridge Electronic Design, Cambridge, UK) and displayed on a PC running Signal software (Cambridge Electronic Design). Nonrecoverable CAP loss from the optic nerve indicates irreversible failure of axon function.[14]

Immunohistochemistry

Rat optic nerves were fixed in 4% paraformaldehyde/0.1 mol/L PBS for 30 minutes before incubation in 0.1 mol/L PBS plus 20% sucrose w/v for 5 minutes and freeze sectioning. In all, 20 μm sections were subsequently blocked for 60 minutes in 0.1 mol/L PBS, 10% normal goat serum plus 0.5% Triton X-100. Sections were then incubated in this solution plus primary antibody overnight at 4°C. Antibodies were raised against: neurofilament-200 (NF-H) and neurofilament-70 (NF-L) (Chemicon, Merck, Temecula, CA, USA; 1:200 and 1:100, respectively), GFAP (1:100, Sigma), Thy-1 (1:100, Santa Cruz, Dallas, TX, USA), pan-NaV (1:100, Sigma), NG-2 (1:100, Upstate, Merck, Temecula, CA, USA) and Nr1 sub-unit of the NMDA GluR (1:100, Santa Cruz). Staining was detected using appropriate Alexa-conjugated secondary antibodies (1:1,000, Cambridge Bioscience, Cambridge, UK). See Salter and Fern[12] for further details of the antibodies used. Primary antibody omission controls were blank. Images were collected using an Olympus confocal microscope (Tokyo, Japan).

Cell Imaging

Live astrocyte imaging was performed on P2 RONs loaded for 60 minutes at room temperature in aCSF containing 10 μmol/L FURA-2-AM. After washing, nerve ends were fixed to a glass coverslip and sealed onto a Plexiglas perfusion chamber (atmosphere chamber; Warner Instruments, Hamden, CT, USA) with silicone grease. Artificial cerebrospinal fluid was run through the chamber (2 to 3 mL/min) and 95% O_2/5% CO_2 was blown over the aCSF. Cells were imaged on a Nikon Eclipse TE200 inverted epifluorescence microscope (Melville, NY, USA). Chamber temperature was maintained closely at 37°C with a combination of flow-through feedback tubing heater (Warner Instruments) and a feedback objective heater (Bioptechs, Butler, PA, USA). Cells were illuminated at 340, 360, and 380 nm (Optoscan monochromator; Cairn Research, Faversham, Kent, UK), and images were collected at 520 nm using an appropriate filter set (Chroma Technology, Bellows Falls, VT, USA). Images were taken with a cooled CCD camera (CoolSNAP HQ; Roper Scientific, Martinsried, Germany) every 60 seconds. Changes in 340:380 ratio were taken to indicate changes in $[Ca^{2+}]_i$. The 360 intensity (isosbestic point) was monitored to assess the capacity of cells to retain dye. The sudden loss of 360 signal correlated with loss of cell membrane integrity and the release of dye into the extracellular space (ECS). See Fern[17] for further details.

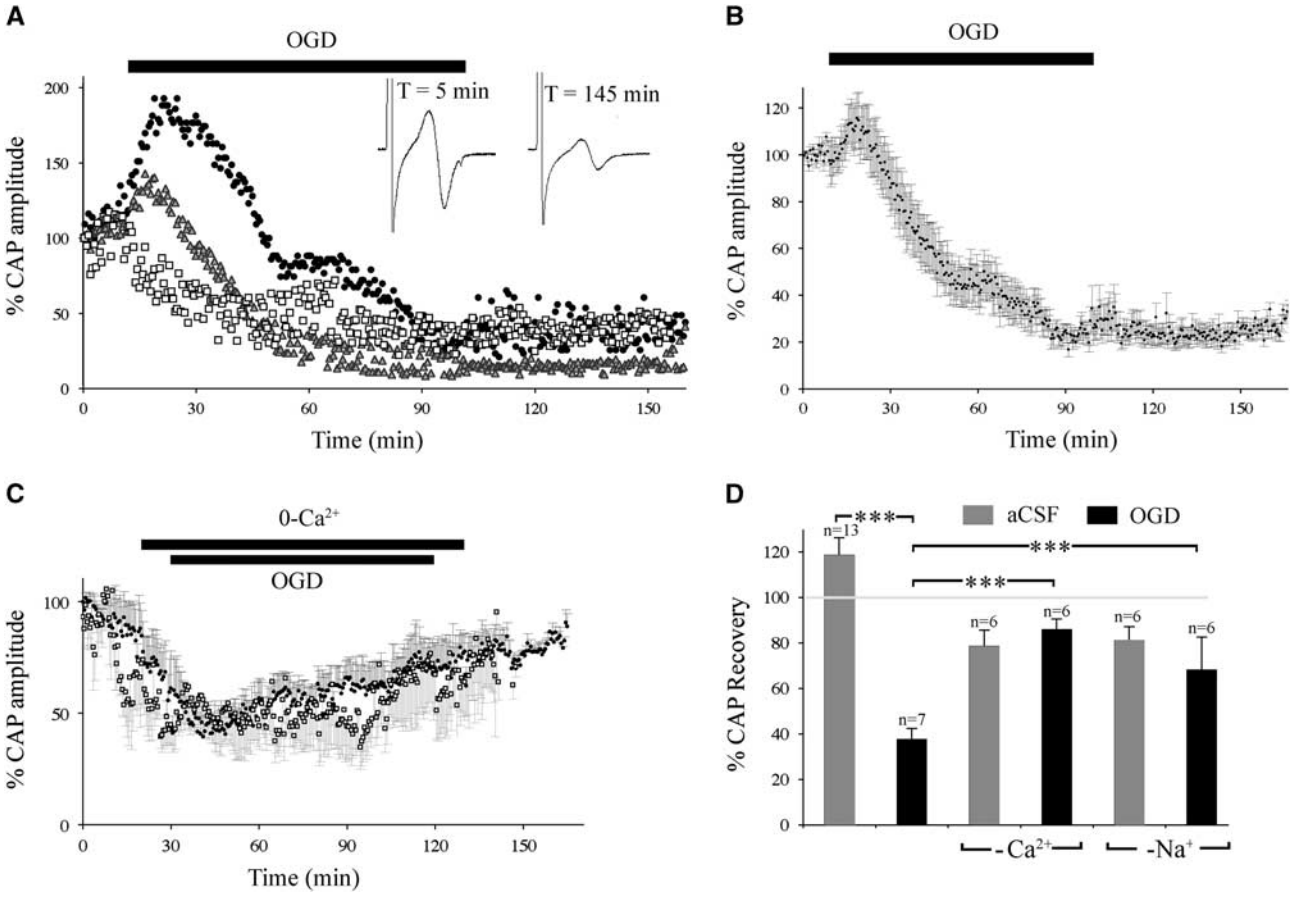

Figure 1. Ischemic injury in premyelinated central white matter. (**A**) Three representative plots of compound action potential (CAP) amplitude in P2 rat optic nerves (RONs) exposed to 90 minutes of oxygen–glucose deprivation (OGD). Note the variable initial rise in CAP amplitude followed by a gradual decline which frequently did not reach zero, followed by the general absence in CAP recovery after reintroduction of artificial cerebrospinal fluid (aCSF). Typical CAP recorded before and after 90 minutes OGD is shown in the inset. (**B**) Mean data showing the effects of 90 minutes OGD perfusion on CAP amplitude. (**C**) The effects of Ca^{2+} removal from the perfusate. Note that under control conditions (filled symbols), zero-Ca^{2+} (indicated by the top bar) evokes a transient CAP decline. In the test experiment (open symbols), OGD has no additional effect than that produce by Ca^{2+} removal alone. (**D**) Data summary showing significantly reduced CAP loss in P2 RON after 90 minutes OGD under either zero-Ca^{2+} or zero-Na^+ conditions (***$P < 0.001$; error bars are s.e.m.).

Electron Microscopy

P2 RONs were washed in Sorenson's buffer and postfixed in 3% gluteraldehyde/Sorenson's. Nerves were fixed (2% osmium tetroxide) and dehydrated before epoxy infiltration. Ultrathin sections were counterstained with uranyl acetate and lead citrate and examined with a Jeol 100CX electron microscope (Welwyn Garden City, UK). Since effectively all axons in the adult RON are myelinated, nonmyelinated axons of the P2 nerve can be considered to be in an early stage of preparation for myelination. For morphometric analysis and viability scoring, axons within a minimum of three grid sections were outlined by hand (Image-J software, NIH) and axon area and perimeter measured. Axon diameter was taken as the mean of the longest and shortest widths. Grids were randomly selected and all identifiable axons within the area were included. Axon viability scores were assigned blind using the following scoring system. Axons were given one point for each of three well-established indicators of viability:[16] (1) the presence of an intact axolemma, (2) the presence of microtubules, and (3) the presence of a debris-free axoplasm. Axons that showed all three attributes were therefore given a viability score of '3', and axons with none were given a score of '0'. Postembedded immuno gold labelling for Nr1 was performed as previously described for P10 RON.[16]

Human Tissue

Tissue from five human fetuses ranging in age between 18 and 23 postconception weeks (PCWs) was studied. Collection of the tissue has been described previously[18] and involved a postmortem delay of 2 to 5 hours after medically induced abortion. Tissue was obtained with signed consent and followed institutional guidelines. In all, 1-mm^3 subcortical blocks were cut from temporal cortex before fixation (1% paraformaldehyde/1.25% glutaraldehyde in PBS) overnight at 4°C. Tissue was then treated as for rat nerve described above, with large ultrathin sections mounted to allow identification of cortical layers and underlying white matter. Immuno-staining for Nr1 protein expression followed previously described protocol.[14]

RESULTS

Ischemic Injury of Premyelinated Central White-Matter Axons

The P2 RON CAP was biphasic and stable under control conditions (Supplementary Figure 1A). Consistent with prior reports,[7] initial experiments showed that a 60-minute period of OGD produced injury in adult RON but failed to damage P2 RON (Supplementary Figure 1B). Longer periods of OGD were tested on P2 RON and a significant CAP loss was produced by a 90-minute challenge. The initial response to OGD at this age was frequently a rise in amplitude that could be as large as 188.3% (e.g., Figure 1A, filled circles), with a mean of 122.0 ± 10.3% after 15.5 minutes of OGD (Figure 1B, $n = 13$). Mean CAP amplitude then decreased pro-

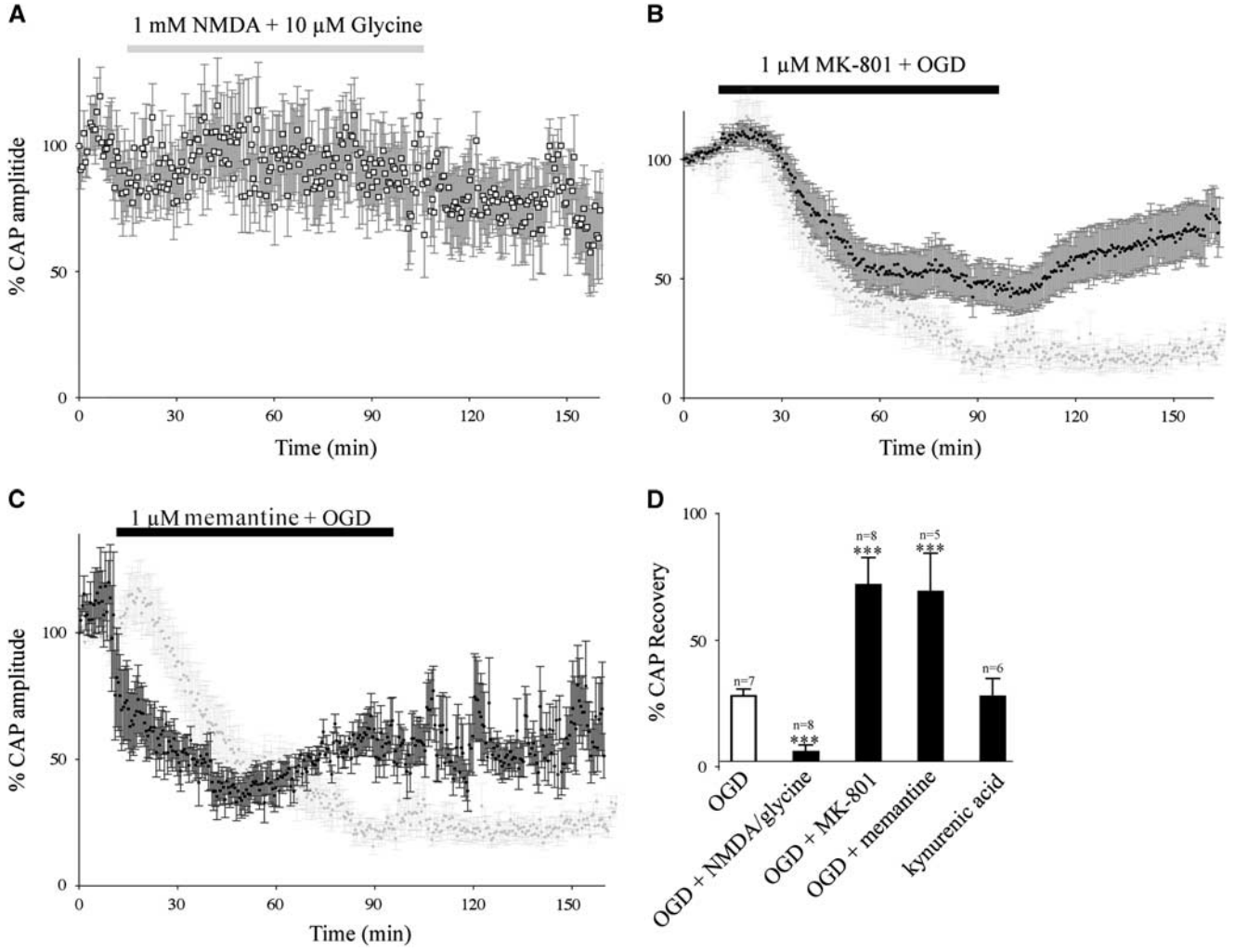

Figure 2. The significance of excitotoxicity. (**A**) *N*-methyl-D-aspartate (NMDA) glutamate receptor (GluR) activation (coperfusion with 1 mmol/L NMDA and 10 μmol/L glycine) for 90 minutes evoked a limited delayed decline in the compound action potential (CAP) under normoxic conditions. (**B**, **C**) NMDA receptor block with 1 μmol/L MK-801 or 1 μmol/L memantine increased recovery from oxygen–glucose deprivation (OGD). (**D**) Data summary showing the effects of NMDA receptor agonists and antagonists on the injury produced by OGD (***$P < 0.001$ versus artificial cerebrospinal fluid (aCSF) of OGD as appropriate).

gressively, reaching 40.3 ± 8.9% of baseline. Unlike white matter from older animals subject to 60 minutes OGD (e.g., Supplementary Figure 1A), P2 RONs exposed to 90 minutes of OGD failed to recover significantly after reinstitution of normoxic conditions (37.5 ± 5.0% after 60 minutes aCSF, $P > 0.05$; Figures 1A and 1B). The absence of recovery after 90 minutes of OGD and the tolerance to 60 minutes OGD indicate progressive and nonreversible conduction failure between these two time points.

Ischemic-type injury of adult RON is both Ca^{2+} and Na^{+} dependent,[19] while at P10 RON injury is Ca^{2+} dependent/Na^{+} independent.[14] This difference is accounted for by the clustered expression of voltage-gated calcium channels on axons in the P10 RON that are yet to initiate myelination.[16] In the P2 RON, CAP declined under zero-Ca^{2+} conditions in otherwise normal aCSF (48.1 ± 12.6% 90 minutes, $n = 6$; Figure 1C), consistent with a large contribution to action potential conduction from voltage-gated calcium channels at this age.[16] This effect was largely reversed when normal aCSF was reinstituted (78.5 ± 7.1%, $n = 6$; Figure 1C). Surprisingly, exposure to 90 minutes OGD 10 minutes after initiating zero-Ca^{2+} conditions, with reintroduction of Ca^{2+} 10 minutes after OGD, resulted in a similar profile of CAP amplitude loss and recovery (Figure 1C, open symbols) to

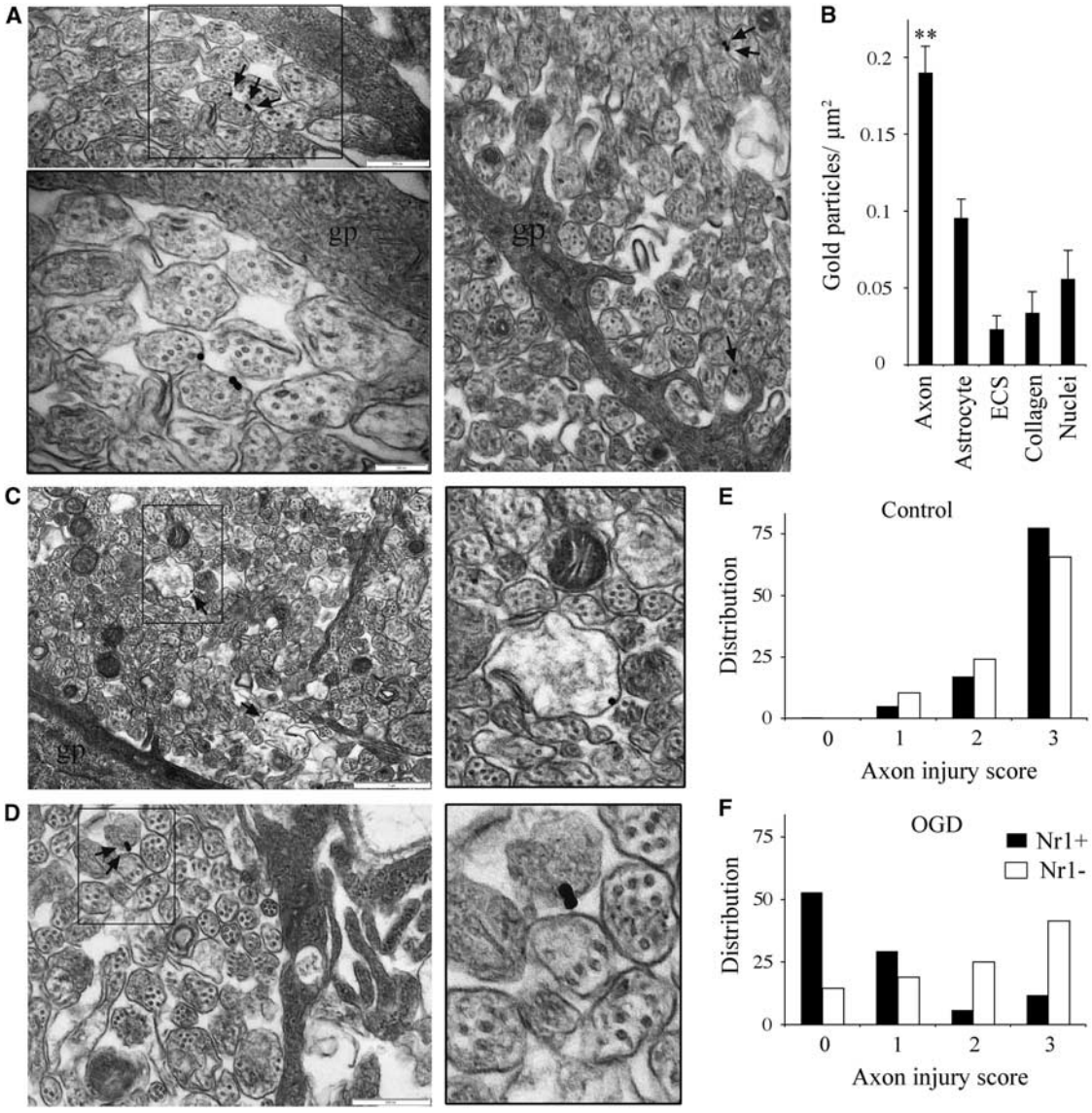

Figure 3. Ultrastructural colocalization of Nr1 on P2 axons correlates with injury. (**A**) Immunolocalization of Nr1 protein in P2 rat optic nerve (RON) (all ultra-micrographs are cross-sections). Left: Axons surround a glial process ('gp'), boxed area shown at high magnification below. Typical axon features are microtubules, vesicular-tubular inclusions, diameter $< 0.4\,\mu m$, and the absence of glial ensheathment. Three gold-particles (arrows) are localized to the axolemma of two neighboring axons. Right: Axons proximal and distal to a glial process have gold particles aligned with the axolemma. (**B**) Blind quantification of gold-particle density in axons, astrocytes, extracellular space (ECS), peri-neural collagen, and glial nuclei. The data show significantly higher staining density in axons versus all other groups (**$P < 0.01$; $n = 7$ nerve sections). (**C**) Nr1 immunolocalization after 90 minutes oxygen–glucose deprivation (OGD)/60 minutes recovery. Axon injury is variable with some axons showing axoplasmic swelling and/or flocculent debris, swollen mitochondria and microtubule loss. Gold particles are localized to the axolemma of badly damaged axon, boxed area shown at high magnification to the right. (**D**) Similar images showing two gold particles localized to the axolemma of a damaged axon. (**E**) Blinded viability scoring of control, showing little pathology and no difference between Nr1 (+) axons and Nr1(−) axons ($n = 400$ axons analyzed from 8 sections). (**F**) A similar analysis after OGD/recovery. Note that viability scores are shifted to lower values for both Nr1(+) axons and Nr1(−) axons, but this effect is greatest in Nr1(+) axons ($n = 398$ axons analyzed).

that seen in zero-Ca^{2+} alone (Figure 1C, filled symbols), suggesting that Ca^{2+}-influx, progressive conduction failure and permanent injury occur over a similar time course under ischemic conditions. Consistent with this, there was no significant permanent loss of the CAP after OGD in zero-Ca^{2+} compared with zero-Ca^{2+} control (85.8 ± 4.7%; Figure 1D). A similar protocol performed under zero-Na^{+} conditions had a similar protective effect (Figure 1D).

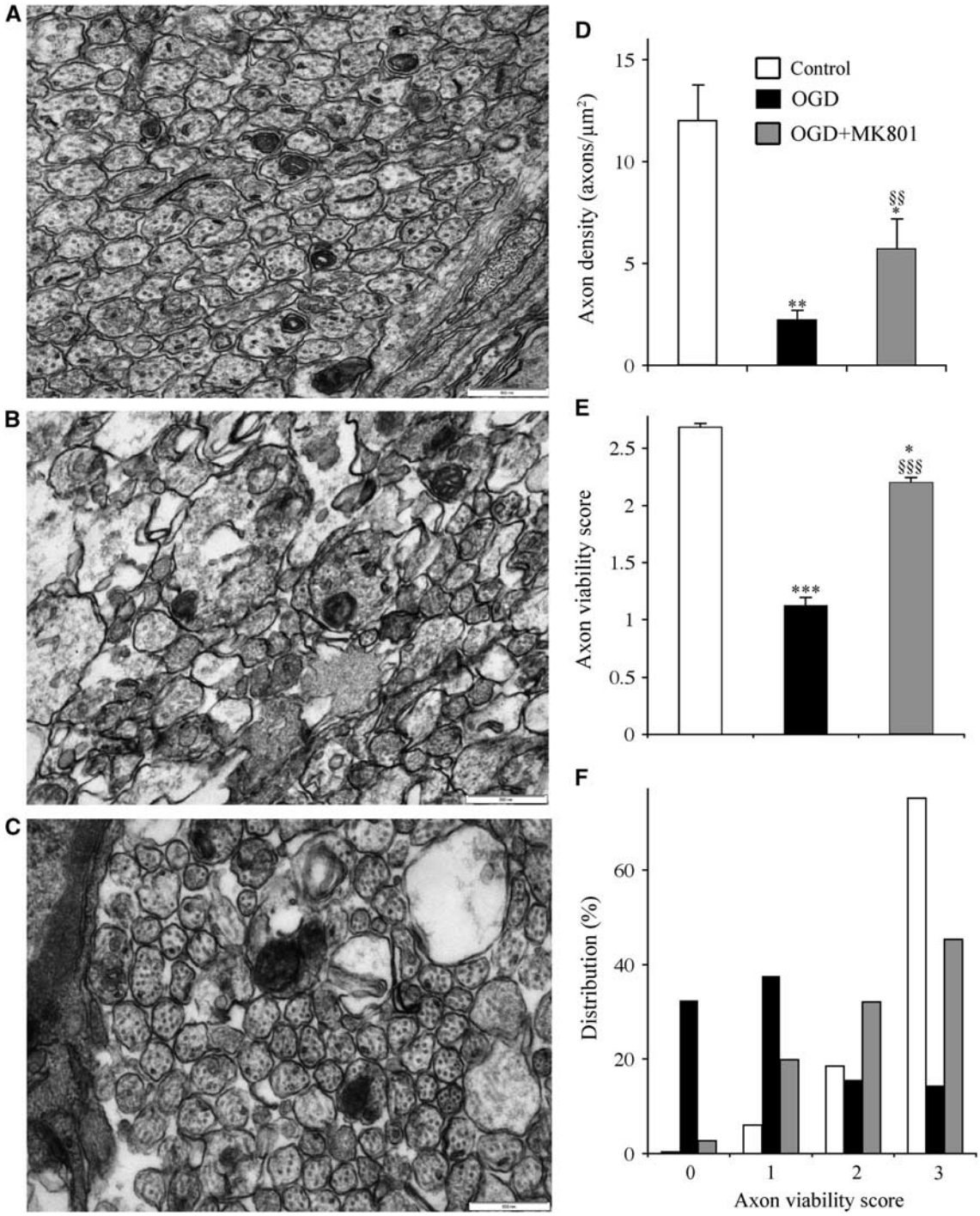

Figure 4. *N*-methyl-D-aspartate (NMDA) receptor block is protective against oxygen–glucose deprivation (OGD)-induced disruption of axon structure. (**A**–**C**) Representative ultramicrographs from control (**A**), post 90 minutes OGD+60 minutes recovery (**B**) and postOGD performed in the presence of 1 μmol/L MK-801 (**C**). (**D**) Blinded counting of axon density in the three groups shows significantly lower number of identifiable axons after OGD ($n = 254$ axons, 6 sections) compared with control perfused rat optic nerves (RONs) ($n = 213$ axons from 5 sections), an effect that was significantly reduced by NMDA receptor block ($n = 576$ axons from 7 sections). (**E**) Blinded axon viability scores were significantly lower in identifiable axons after OGD ($n = 398$ axons from 6 sections), compared with RONs continually perfused with aCSF ($n = 298$ axons from 6 sections), an affect that was prevented by NMDA receptor block ($n = 327$ axons from 6 sections). (**F**) The distribution of axon viability scores in these three conditions, showing that NMDA receptor block restores a more normal pattern of viability. Scale bar = 0.5 μm. '*' = $P < 0.05$ versus control; '**' = $P < 0.01$ versus control; '***' = $P < 0.001$ versus control; $^{§§} = P < 0.01$ versus OGD; $^{§§§} = P < 0.001$ versus OGD.

The Role of Ionotropic Glutamate Receptors

Application of the excitotoxin kainic acid (30 μmol/L: Supplementary Figure 2A) or the NMDA GluR coagonists NMDA (1 mmol/L) +glycine (10 μmol/L: Figure 2A) had no permanent significant effect on the CAP recorded from P2 RON (103.4 ± 7.6%, $n = 6$ and 88.4 ± 11.1%, $n = 7$ of initial CAP area, respectively). Similar findings have been reported in P10[14] and adult[20] RON and these current and prior observations suggest that GluR-mediated injury does not proceed rapidly in the presence of O_2 and glucose. However, we found significant potentiation of OGD-induced injury by superfusion with NMDA+glycine (Figure 2D) and perfusion with the NMDA GluR antagonists MK-801 (1 μmol/L) or memantine (1 μmol/L) resulted in significant protection against OGD (Figures 2B and D). The less specific glutamate antagonist kynurenic acid had no effect either upon control CAPs or the response to OGD (Supplementary Figure 2B).

N-methyl-D-aspartate Glutamate Receptor Expression and Axon Injury

Expression of the obligatory NMDA GluR Nr1 subunit was probed in P2 RON. At the light level, costaining for the astrocyte marker GFAP revealed a degree of colocalization (Supplementary Figure

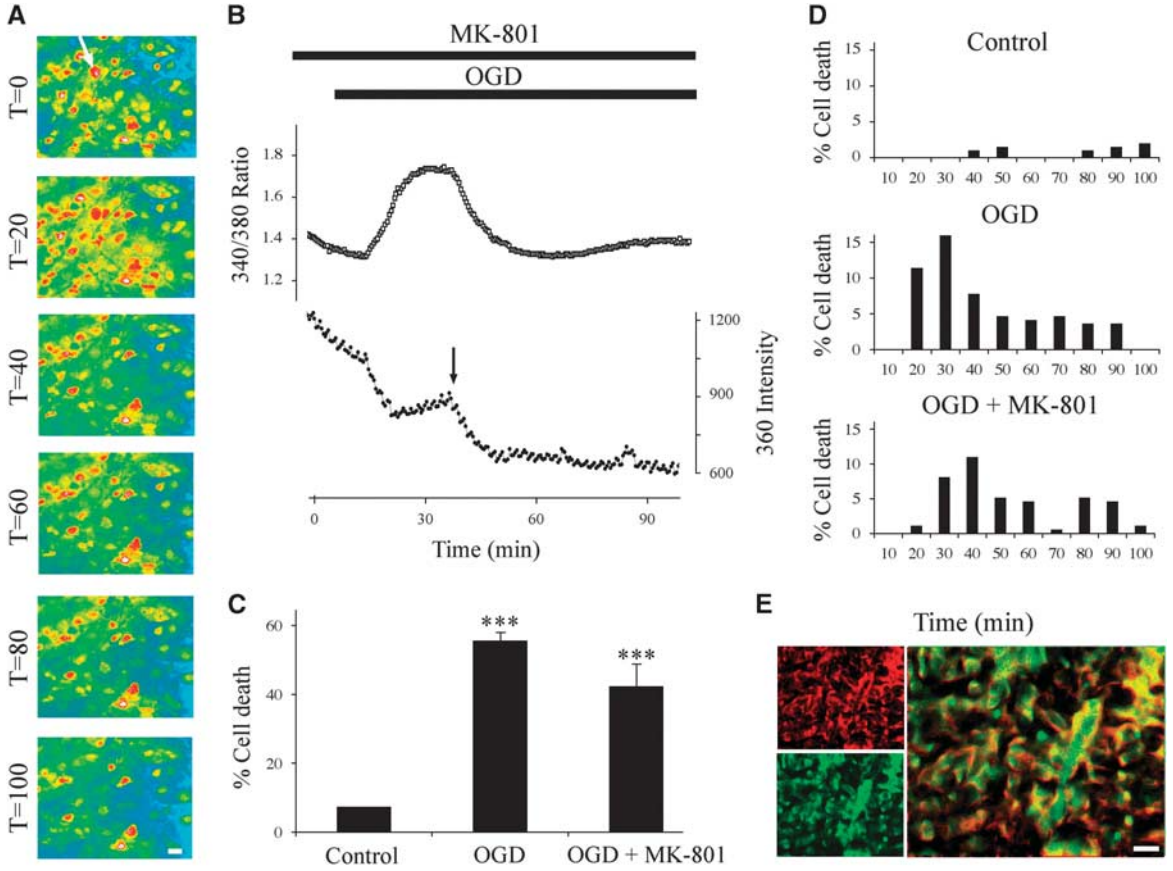

Figure 5. *N*-methyl-D-aspartate (NMDA) receptors do not mediate Ca^{2+} influx or cell death in P2 rat optic nerve (RON) astrocytes. (**A**) FURA-2-AM loaded astrocytes in P2 RON at various times after the onset of oxygen–glucose deprivation (OGD) in the presence of 1 μmol/L MK-801 (arrow indicates cell shown in **B**). (**B**) Changes in 340/380 ratio corresponding to $[Ca^{2+}]_i$ in a representative cell (open squares, top data set, left-hand scale). Note the elevation in 340/380 ratio after the onset of OGD in the presence of MK-801. The 360 intensity of this cell is also plotted (filled circles, lower data, right hand scale). Note the collapse in 360 intensity (arrow), indicative of cell lysis. (**C**) The extent of cell death in P2 RON astrocytes under control conditions ($n = 198$ cells from 6 nerves), during 90 minutes of OGD ($n = 173$ cells from 6 nerves) and during 90 minutes of OGD in the presence of MK-801 ($n = 192$ cells from 6 nerves). Note the significant rise in cell death during OGD compared with control, and the absence of protection in the presence of MK-801 (***$P < 0.001$ versus control). (**D**) Histograms showing the times when cell death occurred under the three conditions. (**E**) GFAP staining (red) and FURA-2 localization (green) in fixed, FURA-2-AM loaded P2 RON. Images overlaid to the right, showing that all FURA-2 filled cells are GFAP(+). Scale = 1 μm.

Figure 6. Glial injury is non-NMDA glutamate receptor (GluR)-R mediated. (**A**) Typical P2 rat optic nerve (RON) astrocyte subjected to 90 minutes OGD/60 minutes recovery shown at low magnification (Top, left) with the three boxed areas at high gain below and to the right. Typical features include glial filaments ('GF'), dark bodies ('db'), and glycogen particles. Golgi apparatus ('ga'), endoplasmic reticulum ('er'), and mitochondria ('Mt') appear intact but swollen. Cell membrane integrity has been lost in this cell (arrows, bottom right panel). (**B**) Dead astrocyte after oxygen–glucose deprivation (OGD)/recovery+1 μmol/L MK-801. The cell has lost membrane integrity and organelles are in continuity with the expanded extracellular space. (**C**) Nerve perimeter after this protocol, showing swollen and severely disrupted astrocyte processes ('*') of the glial limitans adjacent to the basement membrane (arrows); boxed area at high magnification below left, showing intact axons with normal mitochondria and microtubules neighboring the grossly swollen and fragmented glial processes. (**D**) Cell injury scoring for control, 90 minutes OGD/60 minutes recovery and following the same protocol in the presence of 1 μmol/L MK-801. Astrocytes show high levels of injury after OGD, and effect that was not reduced by MK-801 ($n = 22$ astrocytes in each group, ***$P < 0.001$ versus control). (**E**) The distribution pattern of injury scores under these three conditions. NMDA, *N*-methyl-D-aspartate.

3A, e.g., arrows in middle panel), but the majority of Nr1 reactivity existed in the spaces between astrocytes (Figure 3A, '*' in middle panel). Note that the large majority of cells in P2 RON are GFAP(+) astrocytes.[21] Omitting Nr1 antibody from the staining protocol resulted in no staining using identical image collection and processing settings (Supplementary Figure 3, right panels). Costaining for Nr1 and the axonal markers NF-L (Supplementary Figure 3B), Thy-1 (Supplementary Figure 3F), and NF-H

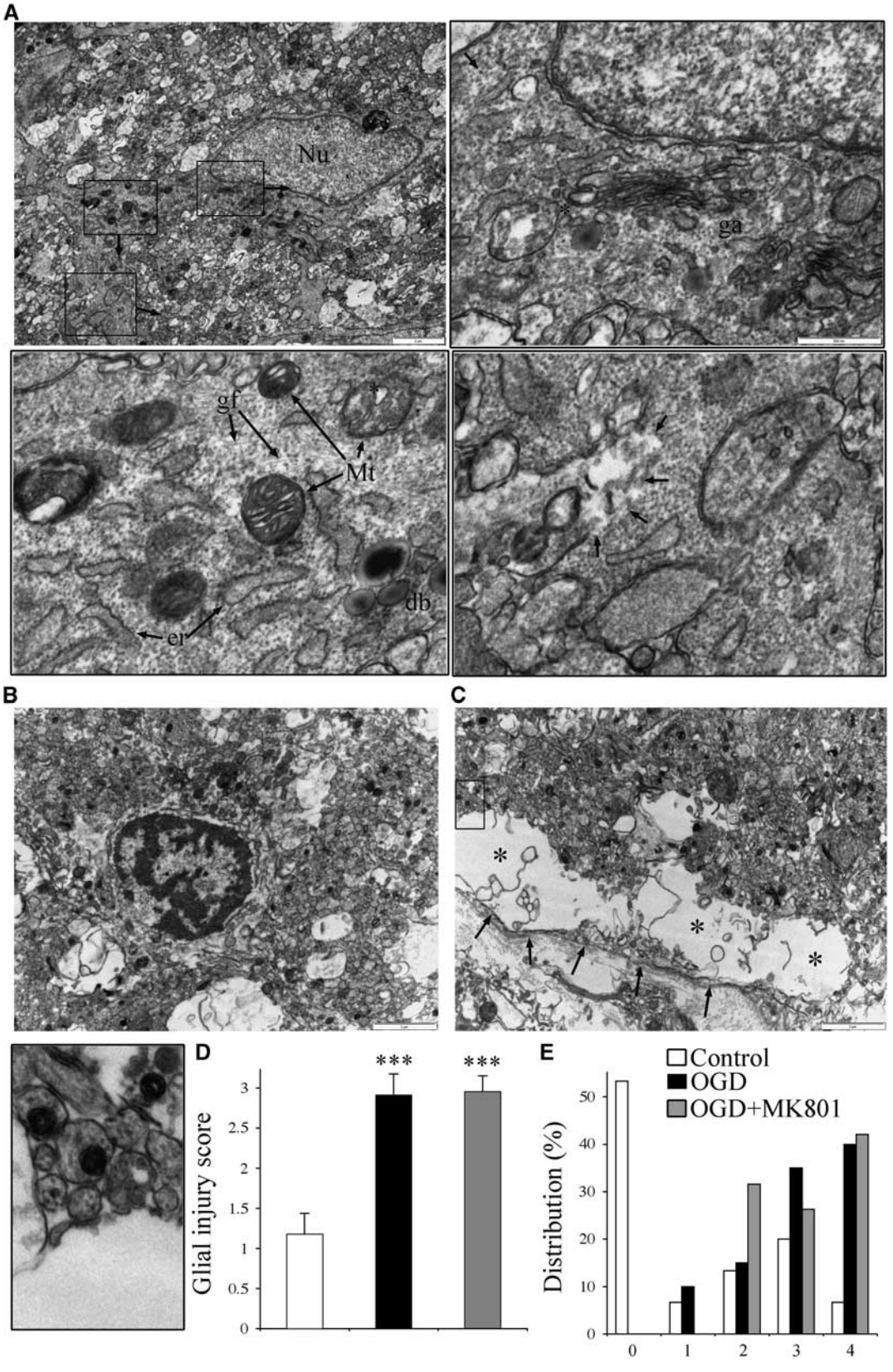

(Supplementary Figure 3G), all showed high levels of colocalization. In the P2 RON, NG-2 staining revealed a population of pericytes aligned along blood vessels that did not express Nr1 (Supplementary Figure 3C). Note, NG-2(+) oligodendrocyte precursors invade the nerve from $>=$P2[22,23] and NG-2(+) cells with the morphology of oligodendrocyte precursors extended processes that were Nr1(+) in P10 RON (Supplementary Figure 3D, arrows), consistent with prior reports.[12,13]

Colocalization of markers at the light level is difficult in a structure like the neonatal RON, where numerous and heterogeneous small structural elements are closely apposed. We therefore used postembedded immuno-gold localization of Nr1 expression at the ultrastructural level to confirm regions of reactivity on axolemma at sites proximal and distal to astrocyte somata and processes (Figure 3A). To assess the selectivity of this staining, gold-particle distribution was assessed throughout six whole sections of P2 RON. Gold particles had a significantly higher density in axons compared with astrocytes and the ECS, and lower densities were found in structures such as collagen fibers of the perineurium and cell nuclei which will represent background levels of staining (Figure 3B).

In P2 RONs subject to 90 minutes of OGD, pathologic changes in the ultrastructure of axons included swelling, loss of microtubules, accumulation of debris in the axoplasm and frank axolemma dissolution (Figures 3C, 3D, and 6). Immuno-gold localization of Nr1 expression was successful in areas of the nerve where axon injury was less extensive (Figures 3C and 3D), revealing frequent reactivity on damaged axons. Staining was also present in more severely damaged regions of the nerve, but it was not possible to ascribe such staining to any specific cell structure and these area are not therefore included in this analysis. The extent of axonal injury in control perfused and postOGD RONs was assessed blind using an established viability scoring system. In control nerves, the mean viability score was 2.72 ± 0.03 (where a score of 3 is no pathology) for Nr1(−) axons ($n = 240$), and 2.55 ± 0.10 for Nr1(+) axons ($n = 58$; $P > 0.05$). The distribution of viability scores was similar for these two groups of axons (Figure 5E). In postOGD nerves, the mean viability score was 1.94 ± 0.18 for Nr1(−) axons ($n = 364$), and 0.77 ± 0.06 for Nr1(+) axons ($n = 34$; $P < 0.001$ versus, Nr1(−) axons). The distribution shows viability scores skewed to low values in the Nr1(+) axons (Figure 3F). The data, therefore, show a strong correlation between sites of high Nr1 reactivity and axon injury.

To analyze the extent of glial and axonal injury after OGD, random high-power fields were collected blind from cross-section ultra-micrographs. Typical fields of axons in control perfused, postOGD and postOGD+MK-801 are shown in Figures 4A and 4C. The density of identifiable axons fell from 12.1 ± 1.8 axons/μm^2 to 2.3 axons/μm^2 afte 90 minutes of OGD+60 minutes recovery ($n = 6$ sections each; $P < 0.01$); with a density of 5.75 ± 1.5 axons/μm^2 after OGD+MK-801 ($n = 6$ sections; $P < 0.01$ versus, control; Figure 4D). The mean viability score of those axons was 2.69 ± 0.03 in control ($n = 298$), 1.12 ± 0.07 after OGD ($n = 398$; $P < 0.001$ versus, control) and 2.20 ± 0.05 after OGD+MK-801 ($n = 327$; $P > 0.05$ versus, OGD alone and < 0.05 versus, control; Figure 4E). This degree of axonal protection against OGD-induced injury is similar to the electrophysiologic protection found in Figure 2D. When the distribution of injury scores was examined, OGD +MK-801 was similar to control (Figure 4F).

Since NMDA GluR Nr1 reactivity was found in some astrocytes at the light level, intracellular [Ca^{2+}] ([Ca^{2+}]$_i$) and cell viability in astrocytes was assessed via FURA-2 cell imaging. As previously reported,[17] FURA-2-AM loading produced dye filling of numerous cells in RON at this age (Figures 5A and 5E). The onset of a 90-minute period of OGD resulted in elevation in the Ca^{2+}-dependent 340/380 ratio in the presence of MK-801 (Figure 5B). Under these conditions, Ca^{2+} rises were frequently followed by breakdown of cell membrane and release of FURA-2 into the extracellular space, apparent as loss of cell fluorescence (e.g., the cell indicated by a white arrow in Figure 5A, which disappears from the image after 40 minutes of OGD; these data are plotted in Figure 5B where cell death is apparent as a sudden decline in the 360 signal indicated by the black arrow). MK-801 did not significantly reduce the extent of cell death produced by OGD (Figure 5C), and did not greatly change the time distribution of cell death (Figure 5D). To ensure that FURA-2 loaded cells were astrocytes, the dye was fixed in whole mount nerves that were subsequently antibody labelled for GFAP (see Fern[17]). This analysis showed that the great majority of FURA-2 loaded cells were GFAP(+) astrocytes (Figure 5E), consistent with the previous observations.[17]

Ultrastructural analysis revealed wide scale swelling of astrocyte organelles (Figure 6A), cell necrosis (Figure 6B) and gross swelling and dissolution of astrocyte processes (Figure 6C) in postOGD +MK-801 P2 RONs. Disruption of astrocyte processes was particularly evident at the nerve perimeter, where the astrocytic elements of the glial limitans neighboring the basement membrane were frequently grossly enlarged with a fragmented cell membrane (e.g., Figure 6C, '*'). In contrast, axons with a normal structure were generally preserved even when surrounded by severely damaged astrocyte processes (Figure 6C, inset). Blinded assessment of astrocyte injury (Figure 6D) and the distribution of injury scores (Figure 6E) confirmed the absence of protection from OGD-induced injury in ultrastructurally identified astrocytes by MK-801.

The incidence of periventricular leukomalacia (PVL) in the human fetus peaks between PCW 23 and 32.[8,24] It is unclear whether axon maturation has initiated in periventricular white matter at the beginning of this period since the major phase of oligodendroglial progression from the O4(-) precursor to O4(+)/O1(−) pre-oligodendrocyte stage does not accelerate until PCW 28.[25,26] In animal models such as the RON, axon diameter expansion initiates several days before the maturation of O4(+) oligodendroglia,[27] and is accompanied by loss of Nr1 reactivity (Figure 3). Formative white matter in fetal intermediate zone at PCW 18 to 23 was therefore analyzed and axons were compared with those of the overlying cortical layers. Axons were readily identified in both regions by their cylindrical structure and the presence of microtubules (Figure 7, e.g., '*'). Axons were generally

Figure 7. Nr1 expression in mid-gestation human cortex. (**A**) Cortical postconception week (PCW) 22 gray matter is rich in small diameter axons (e.g., '*') surrounding larger cell processes ('P') and neuron soma ('N'). Note the characteristic microtubules within axons. Regions of intense reactivity (arrows) are evident within axolemma (boxed areas at high gain to the right), in addition to staining within the neuron and processes. Scale = 1 μm. (**B**–**G**) Subcortical intermediate zone. (**B**) Typical axonal staining of small diameter axons mainly in long section, and cell processes that may be glial. Scale = 500 nm. (**C**) A localized region of intense Nr1 reactivity within the axoplasm underlying a region of axon extension, where the axolemma protrudes from the axon (longitudinally oriented microtubules identify the axon). Scale = 500 nm. (**D**) Axolemma gold staining at the site of glial contact (note axonal microtubules). Scale = 500 nm. (**E**) Gold staining within the axoplasm of an axon, Scale = 500 nm. (**F**) Staining within the cytoplasm of two glial cells ('A'). Cell identification is difficult but the nuclear morphology suggests they are astroglial. (**G**) An astrocyte process identified by glial filaments (e.g., arrow heads) is Nr1(+) (arrows). Scale = 500 nm. (**H**) Reactivity within the cytoplasm and cell membrane of two neighboring glioblasts. Scale = 1 μm. (**I**) Gold particle density in positively identified axons, glia somata, and cell processes in the intermediate zone. Counts were collected from 12 sections, '***' = $P < 0.001$ versus axon density.

found in clusters embedded within fields of larger, less electron dense and less cylindrical processes that contain either a few tubular or filamentous elements (Figure 7, 'P;) that may be growth cones, or contained glial filaments identifying them as astrocyte processes (Figure 7G, 'AP'). In formative gray-matter layers of the cortex, neurons (Figure 7A, 'N') were often densely packed around small fields of processes. Gray-matter axons at this stage were rarely larger than 1 μm in diameter and most were in the 100- to

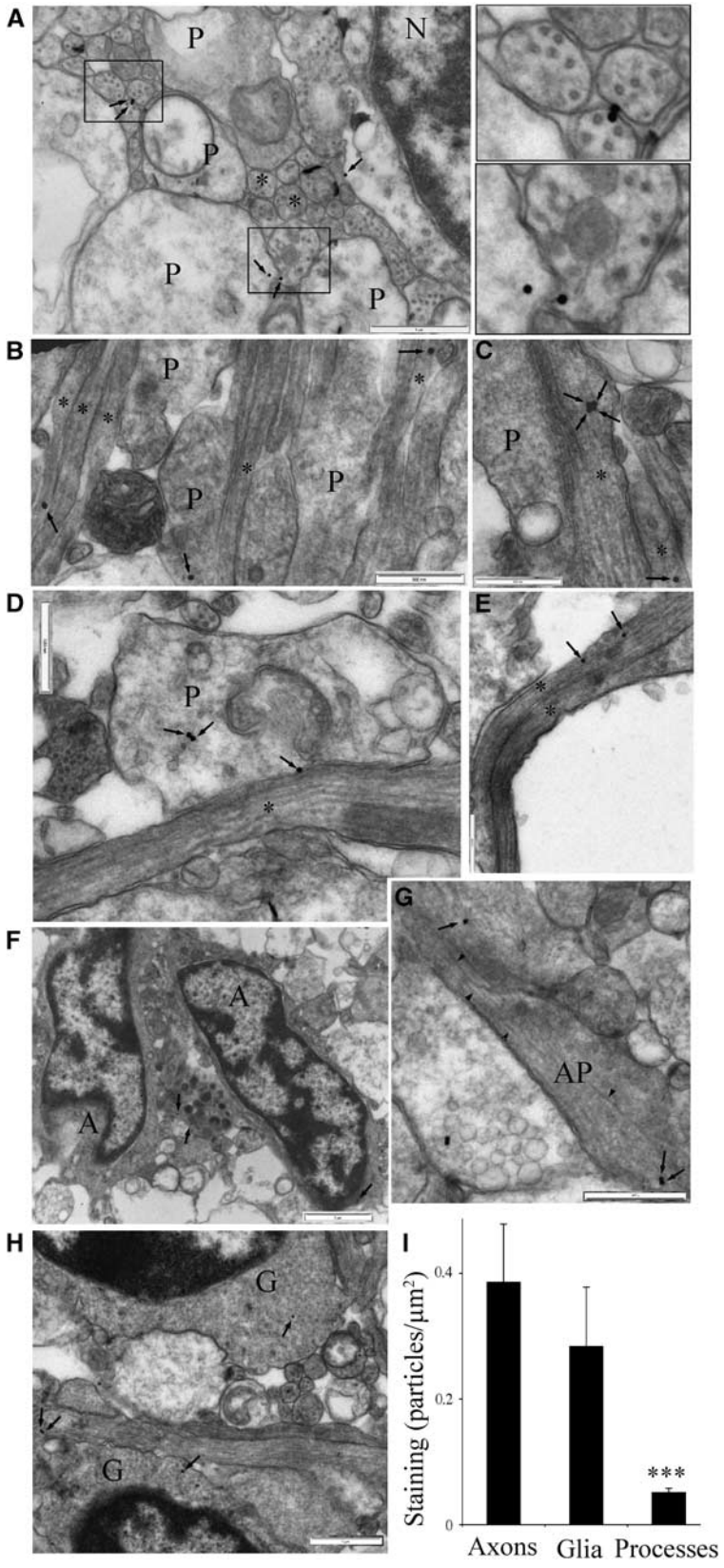

200-nm range (Figure 7A, e.g., '*'). Astrocytes (Figure 7F, 'A') and occasional glioblasts (Figure 7H, 'G') populated the underlying intermediate zone were axons were observed in both cross-section and long-section with axon diameters under 400 nm (Figures 7B and 7H).

Postembedded immuno-gold labelling for Nr1 revealed reactivity in both putative gray-matter and white-matter axons at this developmental stage (Figure 7, e.g., arrows). Axonal staining was generally located within the axolemma in both regions, but axoplasmic staining was also observed (Figures 7B, 7C, and 7E). Staining was observed on occasion at sites where axons extended small hillock-like structures (Figure 7C, four arrows), and at sites where cell processes came into close apposition with axons (Figure 7D). Reactivity was also seen in astrocyte somata (Figure 7F), unidentified processes (Figure 7D), identifiable astrocyte processes (Figure 7G), and glioblasts (Figure 7H). Immunogold staining density for each structure type was calculated for all gold particles in whole grid sections ($n = 8$ sections), revealing significantly higher density in axons and glial cell somata compared with processes (Figure 7I).

DISCUSSION

The formative white matter of the early mid-gestation fetus is composed of radial glial elements, immature axons, navigating growth cones, glioblasts, and astrocytes.[25,28–34] This mix of cellular elements is subjected to ischemic-type lesions such as PVL and diffuse periventricular white-matter injury. The incidence of PVL is elevated between PCW 23 and 32 while diffuse injuries are a common sequelae of very premature birth.[8,24,35] Loss of axon function is the ultimate white-matter deficit in these patients, whether after direct axonal injury[9] or hypomyelination,[36,37] and may result in the common birth disorder cerebral palsy and a range of cognitive deficits.[35] Oligodendroglial lineage progression to the preoligodendrocyte stage accelerates from PCW 28,[25,26] and it has been assumed that premyelinated axon diameter expansion initiates immediately before this key pathophysiologic event, as it does in other mammals.[27] Recent findings suggest that axon diameter expansion above 400 nm is sufficient to initiate axon wrapping,[38] a threshold we show has not been reached by PCW 18 to 23. Occasional myelination has been observed from ~23 to 30 PCW[25,26] and proceeds for years postpartum.[39] A large population of small premyelinated axons therefore populate periventricular white matter until axon ensheathment peaks; a period spanning the windows of heightened susceptibility to all forms of neonatal white-matter injury from PVL to neonatal stroke.

Direct Injury of Small Premyelinated Axons

Axon destruction is a defining feature of focal necrosis in cystic PVL, where severed axon elements are widely described. The incidence of cystic PVL has declined in the West and noncystic PVL has become the predominate form, which may incorporate widespread gliosis punctuated by microinfarcts.[9] Axonal injury assessed via fractin or amyloid precursor protein staining together with imaging studies suggests extensive axonal damage in areas of diffuse gliosis, in addition to within microinfarcts.[9,40–43] The significance of axon loss in noncystic cases may have declined since 2000,[37] and recent studies using *in vivo* models vary significantly in the degree to which they report axon damage.[11,44] Drobyshevsky *et al*[11] in particular point to selective loss of premyelinated central axons in the development of hypertonia in cerebral palsy.

In addition to direct axon injury in focal and possibly diffuse white-matter pathology, the injury pathway described in the Results may be significant for the longer-term viability of surviving axons and their neighboring elements. For example, immature axons contain glutamate in both vesicular and axoplasmic pools,[16,45] and can act as a primary source for excitotoxic glutamate release.[46] Glutamate release from small premyelinating axons may occur during sublethal activation of axonal NMDA GluRs after axoplasmic rises in Ca^{2+}/Na^{+} and the associated axon swelling and vesicle docking; initiating injury pathways on adjacent oligodendroglia. Similarly, sublethal injury to axons at this early developmental stage is likely to disrupt their proper maturation, leading to delayed axon pathology and/or dystrophic axon-glial signalling.

In actively myelinating white matter (P10 RON), oligodendrocyte processes and adjacent small premyelinated axons are sensitive to NMDA GluR-mediated injury.[14] Immuno electron microscopic localization of Nr1 subunit protein to these processes indicates that the primary injury is to the glial elements with secondary injury to small axons, consistent with the rapid injury in P10 RON compared with the earlier stage white matter studied here. Very immature white matter lacks axo-glial junctions and has an expanded extracellular space, allowing unambiguous localization of Nr1 subunit to the axolemma; while the limit of resolution (~15 to 30 nm[47]), makes discrimination between axolemma and glial cell membrane problematic at latter ages. The current findings suggest that NMDA GluR on the smallest, most immature premyelinating axons may contribute to injury in actively myelinating white matter and argue against the actions of an intermediate released from damaged glial processes onto neighboring axons.[14] Once axons initiate diameter expansion, any sensitivity to NMDA GluR-mediated injury is masked by a transient heightened sensitivity to ischemic injury mediated by expression of clustered voltage-gated calcium channels,[15,16] a stage insensitive to NMDA GluR blockers.[14]

Human Early Mid-Gestation Axons

The ultrastructural features of mid-gestation human formative white-matter axons have not previously been described, and the maturation stage of axons in the tissue has only been inferred in earlier studies.[31] We report numerous identifiable small diameter axons in this clinically important tissue, with no axons with a diameter of larger than 400 nm and no ensheathed axons. The RON model allowed delineation of the injury mechanisms operating in the smallest premyelinated axons. NMDA GluR expression was localized to the axolemma and mediated acute cytotoxic Ca^{2+}/Na^{+} influx in a manner similar to that found in oligodendroglial processes[12] and mature neurons. Protection was afforded by competitive and noncompetitive NMDA GluR blockers but not by the nonspecific antagonist kynurenic acid, which acts at the glycine site of the NMDA GluR and has limited anti-excitotoxic action (e.g., Fatokun *et al*[48]).

Nr1 GluR subunit expression examined by quantitative immuno-gold postembedding EM revealed high levels of focal reactivity in small premyelinated axons of formative white matter in the PCW 18 to 23 fetus. Previous light-level studies have shown reactivity in O4(+) oligodendroglia throughout mid-gestation, in addition to levels of background staining consistent with axonal expression.[49] When studied in a rat PVL model, significant white-matter protection was produced using memantine,[49] and the current findings indicate the potential of a similar approach for human cases after early diagnosis.

DISCLOSURE/CONFLICT OF INTEREST

The authors declare no conflict of interest.

ACKNOWLEDGMENTS

The authors thank Ms Natalie Allcock for excellent technical assistance in electron microscopy. The support of the Libyan (TH) and Saudi Arabian (BA) government is gratefully acknowledged as are the comments on the manuscript by James Alix. Professor Nada Zecevic of the University of Connecticut Health Center was generous with provision of fetal tissue and for her comments on the manuscript. Professor

Richard Reynolds and Dr Djordje Gveric are thanked for help in supplying MS tissue from the Multiple Sclerosis and Parkinson's Tissue Bank held at Imperial College London.

REFERENCES

1 Schmitz Y, Luccarelli J, Kim M, Wang M, Sulzer D. Glutamate controls growth rate and branching of dopaminergic axons. *J Neurosci* 2009; **29**: 11973–11981.
2 Ehlers MD, Fung ET, O'Brien RJ, Huganir RL. Splice variant-specific interaction of the NMDA receptor subunit NR1 with neuronal intermediate filaments. *J Neurosci* 1998; **18**: 720–730.
3 Herkert M, Rottger S, Becker CM. The NMDA receptor subunit NR2B of neonatal rat brain: complex formation and enrichment in axonal growth cones. *Eur J Neurosci* 1998; **10**: 1553–1562.
4 Wang PY, Petralia RS, Wang YX, Wenthold RJ, Brenowitz SD. Functional NMDA receptors at axonal growth cones of young hippocampal neurons. *J Neurosci* 2011; **31**: 9289–9297.
5 Aoki C, Venkatesan C, Go CG, Mong JA, Dawson TM. Cellular and subcellular localization of NMDA-R1 subunit immunoreactivity in the visual cortex of adult and neonatal rats. *J Neurosci* 1994; **14**: 5202–5222.
6 Dean JM, Fraser M, Shelling AN, Bennet L, George S, Shaikh S *et al.* Ontogeny of AMPA and NMDA receptor gene expression in the developing sheep white matter and cerebral cortex. *Brain Res Mol Brain Res* 2005; **139**: 242–250.
7 Fern R, Davis P, Waxman SG, Ransom BR. Axon conduction and survival in CNS white matter during energy deprivation: a developmental study. *J Neurophysiol* 1998; **79**: 95–105.
8 Back SA. Perinatal white matter injury: the changing spectrum of pathology and emerging insights into pathogenetic mechanisms. *Ment Retard Dev Disabil Res Rev* 2006; **12**: 129–140.
9 Volpe JJ. Brain injury in premature infants: a complex amalgam of destructive and developmental disturbances. *Lancet Neurol* 2009; **8**: 110–124.
10 Babcock MA, Kostova FV, Ferriero DM, Johnston MV, Brunstrom JE, Hagberg H *et al.* Injury to the preterm brain and cerebral palsy: clinical aspects, molecular mechanisms, unanswered questions, and future research directions. *J Child Neurol* 2009; **24**: 1064–1084.
11 Drobyshevsky A, Jiang R, Lin L, Derrick M, Luo K, Back SA *et al.* Unmyelinated axon loss with postnatal hypertonia after fetal hypoxia. *Ann Neurol* 2014; **75**: 533–541.
12 Salter MG, Fern R. NMDA receptors are expressed in developing oligodendrocyte processes and mediate Injury. *Nature* 2005; **438**: 1167–1171.
13 Karadottir R, Cavelier P, Bergersen LH, Attwell D. NMDA receptors are expressed in oligodendrocytes and activated in ischaemia. *Nature* 2005; **438**: 1162–1166.
14 Alix JJ, Fern R. Glutamate receptor-mediated ischemic injury of premyelinated central axons. *Ann Neurol* 2009; **66**: 682–693.
15 Alix JJ, Zammit C, Riddle A, Meshul CK, Back SA, Valentino M *et al.* Central axons preparing to myelinate are highly sensitivity to ischemic injury. *Ann Neurol* 2012; **72**: 936–951.
16 Alix JJ, Dolphin AC, Fern R. Vesicular apparatus, including functional calcium channels, are present in developing rodent optic nerve axons and are required for normal node of Ranvier formation. *J Physiol* 2008; **586**: 4069–4089.
17 Fern R. Intracellular calcium and cell death during ischemia in neonatal rat white matter astrocytes in situ. *J Neurosci* 1998; **18**: 7232–7243.
18 Zecevic N. Synaptogenesis in layer I of the human cerebral cortex in the first half of gestation. *Cereb Cortex* 1998; **8**: 245–252.
19 Stys PK, Waxman SG, Ransom BR. Ionic mechanisms of anoxic injury in mammalian CNS white matter: role of Na+ channels and Na(+)-Ca^{2+} exchanger. *J Neurosci* 1992; **12**: 430–439.
20 Tekkok SB, Ye Z, Ransom BR. Excitotoxic mechanisms of ischemic injury in myelinated white matter. *J Cereb Blood Flow Metab* 2007; **27**: 1540–1552.
21 Mi H, Barres BA. Purification and characterization of astrocyte precursor cells in the developing rat optic nerve. *J Neurosci* 1999; **19**: 1049–1061.
22 Small RK, Riddle P, Noble M. Evidence for migration of oligodendrocyte--type-2 astrocyte progenitor cells into the developing rat optic nerve. *Nature* 1987; **328**: 155–157.
23 Skoff RP, Price DL, Stocks A. Electron microscopic autoradiographic studies of gliogenesis in rat optic nerve. II. Time of origin. *J Comp Neurol* 1976; **169**: 313–334.
24 Khwaja O, Volpe JJ. Pathogenesis of cerebral white matter injury of prematurity. *Arch Dis Child Fetal Neonatal Ed* 2008; **93**: F153–F161.
25 Back SA, Luo NL, Borenstein NS, Levine JM, Volpe JJ, Kinney HC *et al.* Late oligodendrocyte progenitors coincide with the developmental window of vulnerability for human perinatal white matter injury. *J Neurosci* 2001; **21**: 1302–1312.
26 Jakovcevski I, Zecevic N. Sequence of oligodendrocyte development in the human fetal telencephalon. *Glia* 2005; **49**: 480–491.
27 Hildebrand C, Waxman SG. Postnatal differentiation of rat optic nerve fibers: electron microscopic observations on the development of nodes of Ranvier and axoglial relations. *J Comp Neurol* 1984; **224**: 25–37.
28 Wierzba-Bobrowicz T, Lechowicz W, Kosno-Kruszewska E. A morphometric evaluation of morphological types of microglia and astroglia in human fetal mesencephalon. *Folia Neuropathol* 1997; **35**: 29–35.
29 Roessmann U, Gambetti P. Astrocytes in the developing human brain. An immunohistochemical study. *Acta Neuropathol* 1986; **70**: 308–313.
30 Jakovcevski I, Filipovic R, Mo Z, Rakic S, Zecevic N. Oligodendrocyte development and the onset of myelination in the human fetal brain. *Front Neuroanat* 2009; **3**: 5.
31 Haynes RL, Borenstein NS, Desilva TM, Folkerth RD, Liu LG, Volpe JJ *et al.* Axonal development in the cerebral white matter of the human fetus and infant. *J Comp Neurol* 2005; **484**: 156–167.
32 Huppi PS, Maier SE, Peled S, Zientara GP, Barnes PD, Jolesz FA *et al.* Microstructural development of human newborn cerebral white matter assessed in vivo by diffusion tensor magnetic resonance imaging. *Pediatr Res* 1998; **44**: 584–590.
33 Buser JR, Segovia KN, Dean JM, Nelson K, Beardsley D, Gong X *et al.* Timing of appearance of late oligodendrocyte progenitors coincides with enhanced susceptibility of preterm rabbit cerebral white matter to hypoxia-ischemia. *J Cereb Blood Flow Metab* 2010; **30**: 1053–1065.
34 Zecevic N, Chen Y, Filipovic R. Contributions of cortical subventricular zone to the development of the human cerebral cortex. *J Comp Neurol* 2005; **491**: 109–122.
35 Back SA, Miller SP. Brain injury in premature neonates: a primary cerebral dysmaturation disorder? *Ann Neurol* 2014; **75**: 469–486.
36 Billiards SS, Haynes RL, Folkerth RD, Borenstein NS, Trachtenberg FL, Rowitch DH *et al.* Myelin abnormalities without oligodendrocyte loss in periventricular leukomalacia. *Brain Pathol* 2008; **18**: 153–163.
37 Buser JR, Maire J, Riddle A, Gong X, Nguyen T, Nelson K *et al.* Arrested preoligodendrocyte maturation contributes to myelination failure in premature infants. *Ann Neurol* 2012; **71**: 93–109.
38 Lee S, Leach MK, Redmond SA, Chong SY, Mellon SH, Tuck SJ *et al.* A culture system to study oligodendrocyte myelination processes using engineered nanofibers. *Nat Methods* 2012; **9**: 917–922.
39 Kinney HC, Karthigasan J, Borenshteyn NI, Flax JD, Kirschner DA. Myelination in the developing human brain: biochemical correlates. *Neurochem Res* 1994; **19**: 983–996.
40 Meng SZ, Arai Y, Deguchi K, Takashima S. Early detection of axonal and neuronal lesions in prenatal-onset periventricular leukomalacia. *Brain Dev* 1997; **19**: 480–484.
41 Hirayama A, Okoshi Y, Hachiya Y, Ozawa Y, Ito M, Kida Y *et al.* Early immunohistochemical detection of axonal damage and glial activation in extremely immature brains with periventricular leukomalacia. *Clin Neuropathol* 2001; **20**: 87–91.
42 Haynes RL, Billiards SS, Borenstein NS, Volpe JJ, Kinney HC. Diffuse axonal injury in periventricular leukomalacia as determined by apoptotic marker Fractin. *Pediatr Res* 2008; **63**: 656–661.
43 Dammann O, Hagberg H, Leviton A. Is periventricular leukomalacia an axonopathy as well as an oligopathy? *Pediatr Res* 2001; **49**: 453–457.
44 Riddle A, Maire J, Gong X, Chen KX, Kroenke CD, Hohimer AR *et al.* Differential susceptibility to axonopathy in necrotic and non-necrotic perinatal white matter injury. *Stroke* 2012; **43**: 178–184.
45 Wilke S, Thomas R, Allcock N, Fern R. Mechanism of acute ischemic injury of oligodendroglia in early myelinating white matter: the importance of astrocyte injury and glutamate release. *J Neuropathol Exp Neurol* 2004; **63**: 872–881.
46 Back SA, Craig A, Kayton RJ, Luo NL, Meshul CK, Allcock N *et al.* Hypoxia-ischemia preferentially triggers glutamate depletion from oligodendroglia and axons in perinatal cerebral white matter. *J Cereb Blood Flow Metab* 2006; **27**: 334–347.
47 Hermann R, Walther P, Muller M. Immunogold labeling in scanning electron microscopy. *Histochem Cell Biol* 1996; **106**: 31–39.
48 Fatokun AA, Smith RA, Stone TW. Resistance to kynurenic acid of the NMDA receptor-dependent toxicity of 3-nitropropionic acid and cyanide in cerebellar granule neurons. *Brain Res* 2008; **1215**: 200–207.
49 Manning SM, Talos DM, Zhou C, Selip DB, Park HK, Park CJ *et al.* NMDA receptor blockade with memantine attenuates white matter injury in a rat model of periventricular leukomalacia. *J Neurosci* 2008; **28**: 6670–6678.

Supplementary Information accompanies the paper on the Journal of Cerebral Blood Flow & Metabolism website (http://www.nature.com/jcbfm)